99mTc-labeled TSPO ligand CB86 targeting macrophages for rheumatoid arthritis SPECT imaging and preliminary evaluation of anti-inflammatory effect

Peng Liu
Zhongshan Hospital Xiamen University
Rongshui Yang
Zhongshan Hospital Xiamen University
Fu Su
Zhongshan Hospital Xiamen University
Zhenyu Hou
Zhongshan Hospital Xiamen University
Wentao Dong
Zhongshan Hospital Xiamen University
Zhide Guo
Xiamen University
Chao Ma
Zhongshan Hospital Xiamen University
Huaibo Li
Zhongshan Hospital Xiamen University
Weixing Wang
Zhongshan Hospital Xiamen University
xinhui su (suxinhuii@163.com)
Zhongshan Hospital Xiamen University https://orcid.org/0000-0003-4355-6052

Research

Keywords: TSPO (translocator protein, 18 kDa), Technetium radioisotope, SPECT imaging, Rheumatoid arthritis, Macrophages, Glucocorticoids

Posted Date: December 12th, 2019

DOI: https://doi.org/10.21203/rs.2.18555/v1

Abstract

Background and Objective

TSPO (translocator protein, 18 kDa) is up-regulated in activated macrophages, and serves as an attractive target for macrophages molecular imaging. Previous studies showed that TSPO radiotracer can visualize arthritis via positron emission tomography (PET). Compared with PET, single photon emission computed tomography (SPECT) has several advantages, such as lower cost and commercial availability. The aim of the present study is to develop the 99mTc-labeled TSPO ligand CB86 as a novel SPECT probe for imaging of rheumatoid arthritis and preliminary evaluating the effectiveness of steroid anti-inflammatory therapy.

Methods

A novel TSPO ligand CB86 was linked to DTPAA and then labeled with 99mTc to obtain 99mTc-DTPA-CB86. The labeling efficiency, radiochemical purity, and stability were determined in vitro. In vitro cellular uptake, efflux and binding affinity of 99mTc-DTPA-CB86 to TSPO were performed on RAW264.7 macrophage cells. The distribution and SPECT studies were conducted on Freund's Adjuvant-Induced Left Arthritis in rats after the injection of 99mTc-DTPA-CB86 with or without co-injection of unlabeled DTPA-CB86.

Result

The radiosynthesis of 99mTc-DTPA-CB86 was completed successfully with the labeling yields and radiochemical purity of 95.86 ± 2.45 % and 97.45 ± 0.69 %, respectively. 99mTc-DTPA-CB86 displayed good stability, which the radiochemical purity was more than > 90%, in the saline or mouse serum at 4 h. It also exhibited high specific TSPO binging in RAW264.7 macrophage cells in vitro. The highest uptake ratio was (36.45 ± 2.18) % at 3 h after incubation, and decreased significantly after adding excessive unlabeled DTPA-CB86. 99mTc-DTPA-CB86 bound to TSPO with low nanomolar affinity (IC50 =0.49 nM) in RAW264.7 cells. The cell efflux study showed that 99mTc-DTPA-CB86 has good cell retention by RAW264.7 cells, with only about 13.99 % (decreased from (33.31 ± 2.34) % to (19.32 ± 2.01) % of total input radioactivity) of 99mTc-DTPA-CB86 efflux observed during 4.5 h to 8 h incubation. Biodistribution studies showed the left inflammatory ankle uptake was 2.35±0.10 %ID/g, and the inflammatory ankle to muscle ratio was 3.01 ± 0.09 at 180 min after injection. Small animal SPET imaging studies revealed that 99mTc-DTPA-CB86 could clearly identify left inflammatory ankle with good contrast at 30-180 min after injection. Uptake of 99mTc-DTPA-CB86 in the inflammatory ankles could be largely blocked by an excess of unlabled DTPA-CB86. Furthermore, 99mTc-DTPA-CB86 accumulation in the left inflammatory ankles significantly decreased in RA rats treated with dexamethasone.

Conclusion

99mTc-DTPA-CB86 can be readily synthesized, clearly visualized arthritis with low background and monitor therapy response of anti-inflammatory therapy, suggesting its potential as a novel promising

molecular probe targeting TSPO for arthritic SPECT imaging. Key words TSPO (translocator protein, 18 kDa); Technetium radioisotope; SPECT imaging; Rheumatoid arthritis; Macrophages; Glucocorticoids.

Introduction

Rheumatoid arthritis (RA) is a chronic autoimmune disease that primarily manifests as synovial inflammation. Persistent synovitis leads to severe progressive joint damage, functional disability, morbidity, and increased mortality (1). Moreover, RA is also a systemic autoimmune disease that can affect many tissues and organs and is associated with other diseases, including infections, malignancies and cardiovascular diseases (2). Today, approximately 1–2% of the world population gets injured with RA, most frequently found in developed countries, such as Europe and North America (3). Women predominantly more often get affected than men with ages ranging from 40 to 60 years (4). The etiology of RA is very complex and has not yet been fully elucidated. It has a wide spectrum of clinical characteristics, variability in disease severity, progression and differences in therapeutic response (5). These heterogeneous phenotypes may indicate that variety of factors can contribute in developing RA, including genetic and environmental factors. Among environmental factors, smoking has by far the strongest association with RA due to smoking cigarette smoke inducing pro-inflammatory immune responses via vimentin (6).

Clinical studies have shown that immunological and inflammatory processes resulting in joint destruction have already been set off at the very beginning of RA (7). Thus, it seems reasonable that therapeutic intervention should start as soon as the diagnostic has been established, with the aim of stopping inflammation before irreversible damage is caused (1). Currently, clinical diagnosis of RA is based on the 2010 classification criteria proposed by the American College of Rheumatology (ACR) / European League Against Rheumatism (EULAR) (8). These criteria include characteristics appearing early in the RA course, level of inflammatory markers (C-reactive protein, CRP and Erythrocyte Sedimentation Rate, ESR) and autoantibodies in serum (Rheumatoid Factor, RF and Anti-citrullinated protein antibodies, ACCP). However, they still are not very sensitive and specific to RA (9). Conventional imaging techniques, including plain radiography, ultrasonography, CT, MRI, has poor sensitivity and specificity in the detection of the inflammatory process that happens in the initial stages of RA because these imaging models are anatomical contexts and are rather limited in identifying a pathological condition in early and very early disease stages (10). Therefore, the development of non-invasive, highly sensitive and specific tests/ imaging techniques is essential for very early detection of RA.

Nuclear medicine imaging provides a large scale opportunity in the diagnosis of diseases. These techniques are based on the detecting of gamma rays emitted from biologically active molecules labeled with radioactive isotopes and allow non-invasive in vivo detection of different physiologic and pathologic processes with high sensitivity and specificity. Thus, nuclear medicine imaging has significant potential for timely diagnosis and adequate follow-up of diseases (11). In clinical practice, ^{99m}Tc-MDP bone SPECT (Single Photon Emission Computed Tomography) and ^{18}F-FDG PET (Positron Emission Tomography) are increasingly used to diagnose inflammatory arthritis including RA. They have high

sensitivity but low specificity. In many cases, distinction between inflammatory and metastatic bone processes may be difficult (11). Mounting data of evidence have shown that macrophages are key effector cells in the pathogenesis of RA (12), since macrophages are the major source of cytokines that contribute to synovial inflammation in early stages of RA, and then bone erosion (13). The increase in the number of macrophages in the synovium is an early hallmark of active rheumatic disease (14). Therefore a specific tracer of such a process would be more specific and possibly also enable an earlier detection of RA. Recently, specific ligands targeting macrophage receptors such as CD20 receptor, interleukin-1 (IL-1) receptor, etc. have been investigated in the patients with RA using ^{99m}Tc-anti-CD20, ^{123}I-IL-1ra and ^{124}I-anti-CD20, illustrating the interest for molecular imaging in this type of pathology (15–17).The drawbacks of probes with antibodies severely hamper their clinical applications due to their large size resulting in slow tumor accumulation and slow clearance from the circulation (18).

The translocator protein 18 kDa (TSPO), previously known as the peripheral-type benzodiazepine receptor (PBR) (19), is located in the outer mitochondrial membrane, where it has a function in cholesterol transport from the outer to the inner mitochondrial membrane as a rate-limiting step in steroid biosynthesis (20). Moreover, TSPO is also involved in apoptosis, cell proliferation, anion transport, regulation of mitochondrial functions and immunomodulation (19). Under normal physiological conditions, TSPO levels in macrophages are very low, but a strong increase in TSPO levels occurs in an activated state of macrophages in response to inflammation (21). Hence, TSPO is considered as a promising biomarker for inflammatory diseases (22). Previous studies showed that PET imaging based TSPO ligands, such as ^{11}C® PK11195, ^{11}C-DPA-713, and ^{18}FDPA-714, can visualize RA (2,23,24). Although PET has higher resolution and sensitivity, SPECT held several advantages over PET including lower cost, more widespread availability, favorable physical and imaging characteristics (γ ray = 140 keV, half-life = 6.02 hours). In additional, the preparation of ^{99m}Tc-labeled tracers is efficient, reproducible, and simple, making it easy for clinical use. Therefore, in the present study, we aimed to develop the ^{99m}Tc-labeled TSPO ligand CB86 as a novel SPECT probe for imaging of rheumatoid arthritis and initially evaluating the effectiveness of steroid anti-inflammatory therapy.

Materials And Methods

General

TSPO ligand CB86 was kindly provided by Professor Xuechuan Hong (Wuhan University School of Pharmaceutical Sciences). All chemicals obtained commercially were used without further purification. Freund’s Adjuvant, Diethylenetriamine- pentaacetic acid anhydride (DTPAA), Tin (II) chloride dehydrate, Phenylmethanesulfonyl fluoride (PMSF), and lipopolysaccharide (LPS) were purchased from J & K Chemical Ltd. (Beijing, China). Anti-TSPO antibodies produced in mouse were obtained from Sigma-Aldrich Shanghai Trading Co Ltd. (Shanghai, China). Goat anti-mouse IgG antibody was obtained from Santa Cruz Biotechnology Inc. (Santa Cruz, California, USA). The eluent Na^{99m}TcO$_4$ were obtained from commercial ^{99}Mo/^{99m}Tc generator (China Institute of Atom Energy). WIZARD 2480 gamma counter from

Perkin-Elmer Inc. (Waltham, MA, USA). CRC-25R Dose Calibrator from Capintec Inc. (Ramsey, New Jersey, USA). Mouse macrophage RAW264.7 cell lines were obtained from the Cell Culture Center of Institute of Basic Medical Sciences of Chinese Academy of Medical Sciences (Beijing, China). Male Wistar rats, aged 6-8 weeks (200 to 300 g), were purchased from the Experimental Animal Center of Xiamen University (Xiamen, China). SPECT imaging studies were performed using a nanoScan-SPECT/CT scanner (Mediso, Budapest, Hungary).

Cell culture

The mouse macrophage RAW264.7 cell lines were cultured in DMEM supplemented with 10% fetal bovine serum (FBS) and 1% penicillin-streptomycin. The cells were maintained in a humidified atmosphere of 5% CO_2 at 37 °C, with the medium changed every two days. A 70-80% confluent monolayer was detached by 0.1% trypsin and dissociated into a single cell suspension for further cell culture.

Quantitative Real-Time PCR (qRT-PCR)

The expression of TSPO mRNA in RAW264.7 cell lines with or without LPS treatment is determined by the qRT-PCR based on the method described earlier (25,26). In short, Total RNA was isolated with Trizol reagent (Invitrogen Life Technologies Inc. Grand Island, New York, USA) according to the manufacturer's instructions. The cDNA was synthesized from 2 μg of total RNA using MMLV transcriptase (Toyobo, Shanghai, China) with random hexamers. qRT-PCR were performed using SYBR Premix Ex Taq (Takara, Dalian, China). The human β-actin gene was used as the endogenous control. All cDNA samples were normalized to the β-actin endogenous control; $2^{-\Delta\Delta CT}$ method was used to calculate the relative quantification of TSPO mRNA expression. Primers used for real-time PCR are listed on Table 1. All qRT-PCRs were performed in duplicate.

Table 1 Primers for real-time PCR.

□□□	□□□□	□□□□
TSPO	GCTGTGGATCTTTCCAGAACA	ATGCCAAGAGGGTTTCTGC
ß-actin	TACCCAGGCATTGCTGACAGG	ACTTGCGGTGCACGATGGA

ß-actin was used as the endogenous control

Western blot analysis

According to the previously described methods (25,26), the expression of TSPO protein in RAW264.7 cell lines with or without LPS treatment is determined by western blot analysis. Shortly, RAW264.7 cells were lysed in 1 mL RIPA solution (containing 1% Triton X-100, 1% deoxycholate, and 0.1% SDS; Beyotime Biotechnology, Haimen, China) supplemented with a protease inhibitor (PMSF, Sangon, shanghai, China) for 30 min at 4 °C, then centrifuged at 12000 rpm for 30 min at 4 °C to obtain the total cell extracts. 15 mL cell extracts were subjected to SDS-PAGE and transferred onto a PDVF membranes by MiniPROTEAN

(Bio-Rad, Hercules, California, USA). The PDVF membranes were blocked with TBST (10 mM pH 7.4 Tris-HCl, 150 mM NaCl, and 0.1% Tween-20) containing 5% skim milk for 2 h at 37 °C, and incubated overnight at 4 °C with anti-TSPO mAb (diluted 1:100). After washed with TBST three times, the membranes were again incubated with goat anti-mouse IgG labeled peroxidase (diluted 1:5000) for 1 h 37 °C. Protein of interest were visualized with ECL in Kodak Image Station 4000R (Carestream Health, Rochester, New York, USA). ß-actin was used as an internal control. All experiments were performed in duplicate.

Cellular immunofluorescence staining

Cellular immunofluorescence staining was performed as previously described (25,27). Briefly, the cell-seeded coverslips were washed and fixed. The TSPO mAb (diluted 1:100) and fluorescence (TRITC)-labeled secondary antibody (diluted 1:50; Gibco, Grand Island, New York, USA) were added restained with Hoechst 33258 (Beyotime Biotechnology, JiangSu, China). The sildes with cells were incubated without the TSPO mAb as control. The fluorescence images were captured at excitation laser of 360 nm and emission laser of 460 nm for Hoechst 33258, and at excitation laser of 488 nm and emission laser of 530 nm for FITC by using Olympus FV 1000 Inverted Confocal Fluorescence Microscope (Olympus, Columbia, South Carolina, USA). All experiments were performed in duplicate.

Cell viability assay

Cell viability was analyzed by MTT assay. RAW264.7 cells and 4T1 cells (with low TSPO expression) were seeded in 96 well plates at 1×10^4 cells and were treated with CB86 or CB86-DTPA suspensions (100 μL per well), respectively, at different concentrations (0, 1.25, 2.5, 5, 10, 20 μM in DMEM) for 24 hours at 37°C and 5% CO2. Subsequently, 10 μL of 5 mg/mL MTT was added to each well and incubated for an additional 4 h at 37 °C under 5% CO_2. The optical density (OD) in each well was measured by a scientific microplate reader (Multiskan Spectrum; Thermo Fisher, USA). The OD at 490 nm was determined. The OD from the wells of the cells cultured with complete medium was taken as 100% viability. Relative cell viability (%) compared to control cells was calculated using the formula: % viability = OD (treated) / OD (control) x 100%.

Synthesis of coumarin-CB86

CB86 purity and molecular mass were determined by analytic scale reversed-phase high-performance liquid chromatography (HPLC, model: 3000 HPLC System, Dionex Corporation, Sunnyvale, California) and matrix-assisted laser desorption/ ionization–time of flight mass spectrometry (MALDI-TOF-MS, model: Perseptive Voyager-DE RP Biospectrometer, Framinghan, Massachusetts). After that, CB86 (50 mg) dissolved in DMSO (2 mL) and 7-Hydroxylcomuarin (1.62 g, 10 mmol) were added to ethanol (140 mL). The reaction mixture was stirred at 60 °C for 30 min and then was cooled to 5 °C in an ice bath. The byproduct was removed by filtration and then purified by column chromatography (hexane/ethyl acetate = 6:1, v/v) to give a white filtrate containing coumarin-CB86.

Fluorescence imaging of CB86 in living cells

The RAW264.7 cells stimulated with LPS were incubated in the probe coumarin-CB86 (25 μM) with or without CB86 (10.0 μg) for 2 h at 37 °C and washed with 0.1 M PBS (0.6 mL x 3) before observation. The cells were then stained for 10 min with MitoRed, a well-established mitochondrial dye. The cells were observed using the confocal fluorescence microscope (Olympus FV 1000 Inverted, Olympus, Columbia, South Carolina, USA) with a 63 × oil-immersion objective lens. The excitation wavelength was 346 nm, and emission was collected at 455±10 nm. All experiments were performed in duplicate.

Conjugation of DTPA-CB86

CB86 (50 mg) and DTPAA (200 mg) were dissolved in DMSO (2 mL) under vigorous stirring and stirred at room temperature for 24 h in the dark. The byproduct was removed by filtration to give a reddish-brown filtrate containing DTPA-CB86. The DTPA-CB86 was characterized by HPLC and MALDI-TOF-MS.

Labeling DTPA-CB86 with ^{99m}Tc

The radiolabeling method of DTPA-CB86 was performed as our previously described methods (28). The compound DTPA-CB86 was labeled with ^{99m}Tc using $SnCl_2{\cdot}2H_2O$ as a reducing agent. Briefly, 100 μg/100 μL of DTPA-CB86 and 20 μL of $SnCl_2$ (2 mg/mL in 0.1 M HCl) were mixed in a vial. Next, 185~370 MBq of freshly $Na^{99m}TcO_4$ was added to the mixture. The reaction mixture was then incubated at 100 °C for 30 min to obtain the resulting radiotracer ^{99m}Tc-DTPA-CB86. The resulting solution of ^{99m}Tc-DTPA-CB86 was purified and analyzed by Sep-Pak C18 cartridge (GE Healthcare, Piscataway, New Jersey), and radio-HPLC (Thermo Scientific, Waltham, MA, USA). The mobile phase is presented below: A: H_2O, B: 100% CH_3OH; 0-10 min, B: 10%; 10-20 min, B: 90%; 20–30 min, B: 90%; 30-40 min, B: 10%; flow rate: 0.5 mL/min. The synthetic scheme of ^{99m}Tc- DTPA-CB86 is shown in Figure 1.

Determination of lipid-water partition coefficient of ^{99m}Tc-DTPA-CB86

To determine the hydrophilicity of ^{99m}Tc-DTPA-CB86, the partition coefficient (expressed as log P) was measured as our previously described methods (28). 200 μL ^{99m}Tc-DTPA-CB86 was added to 1 mL phosphate-buffered saline (PBS, pH = 7.4) saturated by n-octyl alcohol and 1 mL n-octyl alcohol saturated by PBS (pH = 7.4). After shaking for 5 min at room temperature, The solution was centrifuged at 3000 rpm for 5 min. Afterward, 100 μL of the organic phase and water phase were counted in a gamma counter, respectively. The averaged activities from each phase were used to calculate the log P values. The lipid-water partition coefficien (Po/w) of ^{99m}Tc-DTPA-CB86 was calculated as (cpm in organic phase)/(cpm in water phase). All the experiments were performed with triplicate samples and reported as mean ± SD.

In *vitro* stability analysis

In vitro stabilities in saline and mouse serum were determined similarly to the procedures previously described with minor modifications (29,30). ^{99m}Tc-DTPA-CB86 (5.55 MBq) in 250 µL of PBS was added to 2.0 mL of saline or mouse serum and was incubated at 37 °C for 1, 2, and 4 h. At each time point, the mixture in the mouse serum 1.85 MBq was precipitated with 300 µL of ethanol and centrifuged at 16,000g for 2 min. The supernatant was transferred to a new Eppendrof tube, and DMF (300 µL) was added to precipitated the residue of serum protein. After centrifugation, the supernatant or the mixture in saline was acidified with 300 µL of buffer A (water + 0.1% TFA) and filtered using a 0.2 -µm nylon Spin-X column (Corning Inc. Corning, New York). The filtrates were then analyzed by radio-HPLC under conditions identical to the ones used to analyze the original radiolabeled compound. The percentage of intact of ^{99m}Tc-DTPA-CB86 was determined by quantifying peaks corresponding to the intact and the degradation products. The assays were repeated twice.

Cell assays

Cell uptake, blocking, and efflux assays were performed as previously described with minor modifications (28-31). Briefly, the RAW264.7 cell lines were cultured in DMEM supplemented with 10% FBS and 1% penicillin-streptomycin. The cells were maintained in a humidified atmosphere of 5% CO_2 at 37 °C, with the medium changed every two days. A 70-80% confluent monolayer was detached by 0.1% trypsin and dissociated into a single cell suspension for further cell culture. All experiments were performed in duplicate.

Cell uptake assay The RAW264.7 cells were washed three times with 0.01 M PBS (pH 7.4) and dissociated with 0.25% trypsin-EDTA. DMEM medium was then added to neutralize trypsin-EDTA. Cells were spun down and re-suspended with serum free DMEM. Cells (0.5×10^6) were incubated at 37 °C for 30, 90, 180, and 240 min with 1.85×10^{-2} MBq 100 µL ^{99m}Tc-DTPA-CB86 in 0.5 mL serum-free DMEM medium. The non-specific binding of the probes with RAW264.7 cells was determined by co-incubation with 10.0 µg unlabeled DTPA-CB86. At each time point, after supernatants were removed, cells were washed with PBS and then lysed with 1 mL NaOH (1 M) for 5 min. The radioactivity of the lysates was measured using a gamma counter, and the cell uptake (counts/min) was normalized to the percentage of binding for analysis using Excel (Microsoft Software Inc., Redmond, Washington). All experiments were performed in duplicate.

Binding affinity assay The RAW264.7cells (0.2×10^6) were plated on 24-well plates one day before the experiment. After washing twice with DMEM, the cells were incubated at 25 °C for 3 h with 1.11×10^{-2} MBq 100µL ^{99m}Tc-DTPA-CB86 in 300 µL of DMEM with concentrations of unlabeled DTPA-CB86 ranging from 10^{-13} to 10^{-5} mol/L. After incubation, the cells were washed with cold PBS three times and detached with 1 mL NaOH (1 M) for 5 min. The radioactivity in the cells was measured using a gamma counter and were corrected for physical decay. The data were analyzed using GraphPad Prism (GraphPad Software Inc. San Diego, California), and the half maximal inhibitory concentration (IC50 value) of ^{99m}Tc-DTPA-CB86 was measured using a least squares fitting routine. All experiments were performed in duplicate.

Cell efflux study The RAW264.7 cells in separate 24 well plates were incubated with 1.11×10^{-2} MBq 100μL ^{99m}Tc-DTPA-CB86 at 37 °C for 240 min. After washing twice with PBS, cells were then incubated with culture medium for 30, 90, 180 and 240 min again to monitor the radioactivity efflux. At each time point, the cells were washed, lysed, and counted using a gamma counter. The cell retention rate of radioactivity was expressed as a percentage of the total input radioactive dose.

Induction of RA, assessment and anti-inflammatory therapy

Induction of RA. Experimental RA was induced in male Wistar rats according to the method previously described with some modifications (2,32). Briefly, the left ankle of each rat was injected with 0.1 mL of Complete Freund's Adjuvant (CFA) with Mycobacterium butyricum 1% suspension in mineral oil.

Assessment of arthritis. The body weight of rats and development of RA disease were supervised daily by two observers. The severity of RA was evaluated according to the following scale: grade 1, detectable swelling in one joint; grade 2, swelling in two joints; grade 3, swelling in three joints; grade 4, severe swelling of the entire paw. The maximum score per animal for the four joints was 16. Each observation was done under short anesthesia using an isoflurane/oxygen mixture (2 to 3%). Each joint was graded, so the maximum score was 16 for a rat. Meanwhile, two weeks after injecting, the joint thickness was measured by a vernier caliper (Exploit Technology CO., LTD., Taiwan, China). Rats were allowed to grow to around grade 2 and 3 and then the RA rats were subject to in vivo biodistribution and imaging studies.

Anti-inflammatory therapy. RA rat with grade 4 (n =4 for each group) were administered with 0.5 mg/kg.d dexamethasone or saline by stomach perfusion once a day for 2 weeks, and then were imaged at the 7th day of and 15th day after treatment, respectively. The saline treated group as control group.

Biodistribution study

The animal procedures were performed according to a protocol approved by the Institutional Animal Care and Use Committee of Zhongshan Hospital Xiamen University. RA rats (n =4 for each group) were injected with ^{99m}Tc-DTPA-CB86 (0.37 MBq, 100μL) through the tail vein. At 30, 90, and 180 min after injection, the mice were sacrificed, and the left inflammatory ankles and normal tissues of interest were removed and weighed, and their radioactivity was measured in a gamma counter. The radioactivity uptake in the left inflammatory ankles and normal tissues were expressed as a percentage of the injected radioactivity per gram of tissue (%ID/g). In order to study the in vivo TSPO targeting specificity of ^{99m}Tc-DTPA-CB86 based on the previous studies (28,29), unlabeled DTPA-CB86 (300 μg) was co-injected with ^{99m}Tc-DTPA-CB86 in RA rats (n =3 for each group) via a tail vein, and biodistribution studies were conducted at 180 min after injection. The radioactivity ratios of the left inflammatory ankle to blood (LIA/B) and the left inflammatory ankle to muscle (LIA/M) were calculated.

SPECT imaging

SPECT imaging of RA rats was performed using a nanoscan SPECT/CT preclinical imager (Mediso, Hungary). The RA rats (n =4 for each group) were injected with ^{99m}Tc-DTPA-CB86 (0.37 MBq, 100μl) with or without co-injection of unlabeled DTPA-CB86 (300 μg) through the tail vein. At 30, 90, and 180 min after injection, the mice were anesthetized with 2% isoflurane and placed on SPECT bed (ventral side down). SPECT acquiring parameters were as follows: 140 keV energy peak for ^{99m}Tc, window width of 20%, matrix of 256 × 256, medium zoom, and frame: 30 s. Whole body static images (200,000 counts) were acquired with a matric of 218 × 218, and zoom of 2.0. CT data were acquired using an X-ray voltage biased to 50 kVp with a 670 μA anode current, and the projections were 720^0. Regions of interest (ROIs) were drawn over the left inflammatory ankle and normal muscle, and then the ratios of the left inflammatory ankle to muscle ((LIA/M) were calculated.

Histological evaluation of the RA model

The left inflammatory ankles, contralateral normal ankles from RA rats were harvested and immediately frozen in dry ice. Thawed tissues were sliced into pieces. Hematoxylin and Eosin (HE staining), and immunohistochemistry (IHC) tests were performed on 5 μm frozen sections of ankle slices.

HE staining was conducted according to routine protocols. Briefly, after deparaffinization and rehydration, 5 μm longitudinal sections were stained with hematoxylin solution for 5 min followed by 5 dips in 1% acid ethanol (1% HCl in 70% ethanol) and then rinsed in distilled water. Then the sections were stained with eosin solution for 3min and followed by dehydration with graded alcohol and clearing in xylene. The mounted slides were then examined and photographed using an Olympus BX53 fluorescence microscope (Tokyo, Japan).

Immunohistochemical staining

The slides were blocked with 5% goat serum in PBS containing 0.1% Triton X-100 for 1 h at room temperature and then incubated with rabbit anti-rat TSPO (1:200, Sigma) antibodies for 2 h at room temperature. After being washed, the slides were then incubated for 2 h at room temperature with secondary antibodies Goat anti-mouse IgG antibody (1:1,000; Sigma).The slides were then examined and photographed using an Olympus BX53 fluorescence microscope (Tokyo, Japan).

Statistical methods

The experimental data were analyzed by SPSS 18.0 (SPSS Company, Chicago, IL, USA). Statistical analysis was performed using two tailed Student's t-test for unpaired data. Data are expressed as mean ± standard deviation and $P < 0.05$ was considered to indicate a statistically significant difference.

Results

Expression of TSPO in the activated RAW264.7 cells

As shown in Figure 1A, qRT-PCR results indicated that the expression of TSPO mRNA in the activated RAW264.7 cells was significantly higher than that in the resting RAW264.7 cells (P <0.01). Consistent with qRT-PCR, Western blot (Figure 1B) demonstrated that the activated RAW264.7 cells exhibited higher levels of TSPO protein expression. Immunofluorescence analysis showed (Figure 2) that TSPO widely over-expressed in activated RAW264.7 cells, and is mainly located in the cytoplasm. These results could be concluded that TSPO is excessively expressed in macrophage RAW264.7 cells induced by LPS.

In vitro cytotoxicity of CB86 and CB86-DTPA

In vitro cytotoxicity of CB86 and CB86-DTPA was determined using the MTT assay in RAW264.7 and 4T1 cells. The cells were incubated with different concentrations of CB86 and CB86-DTPA for 24 hours, respectively. As shown in Figure 3, the cell survival rates of RAW264.7 and 4T1 cells were not significantly different (P > 0.05) between the groups of CB86 and CB86-DTPA. The cell survival rates were > 90% even in the concentration of 20 μM CB86 and CB86-DTPA, indicating that CB86 and CB86-DTPA were safe to the RAW264.7 and 4T1 cells at the test concentrations.

Fluorescence imaging of CB86 in the activated RAW264.7 cells

As shown in Figure 3, the activated RAW264.7 cells were stained with MitoRed a well-established mitochondrial dye, and subjected to confocal fluorescence microscopy. CB86-coumarin was found to be localized to mitochondria (Figure 4A), whereas, it was barely observed in the presence of CB86 (Figure 4B). These results indicated that CB86 could bind well with TSPO receptor on the surface of mitochondrion in the activated RAW264.7cells.

Radiosynthesis of ^{99m}Tc-DTPA-CB86 and log P determination

The radiosynthesis of ^{99m}Tc-DTPA-CB86 is shown in Figure 5. The retention times of CB86 and DTPA-CB86 on analytical HPLC were found to be 15.31 min and 24.72 min, respectively. The measured molecular weight (MW) of CB86 and DTPA-CB86 on MALDI-TOF-MS was 384.53 and 759.03, respectively (calculated MW=384.17 and 759.3, respectively). The MW for its construct was consistent with the expected MW.

^{99m}Tc-DTPA-CB86 was successfully radiosynthesized. Under radio-HPLC conditions described above, ^{99m}Tc-DTPA-CB86 showed a retention time of 25.7min. The radiolabeling efficiency, radiochemical purity and specific activity of ^{99m}Tc-DTPA-CB86 were 95.86±2.45%, 97.45±0.69%, and 2.6 MBq/nmol, respectively. The lipid-water partition coefficient (log P) of ^{99m}Tc-DTPA-CB86 is -1.22±0.04, suggesting ^{99m}Tc-DTPA-CB86 is a water- soluble compound.

In *vitro* stability analysis

In *vitro* stability studies (Figure 6, 7) showed that more than 90% of ^{99m}Tc-DTPA -CB86 remained intact during 1 to 4 h of incubation in the saline or mouse serum, indicating that ^{99m}Tc-DTPA-CB86 maintained

excellently stable in the saline or mouse serum.

Cell assays

Cell uptake ratios of ^{99m}Tc-DTPA-CB86 were shown in Figure 8A. ^{99m}Tc-DTPA- CB86 accumulated in RAW264.7 cells and reached a highest value of 36.45±2.18% of applied activity at 180 min. When the probe was incubated with large excesses of non-radioactive DTPA-CB86, its uptake levels in RAW264.7cells was significantly inhibited (P<0.05) at all incubation time points.

The binding affinity of ^{99m}Tc-DTPA-CB86 to TSPO was determined through the receptor saturation assay. As shown in Figure 8B, the IC_{50} value of ^{99m}Tc-DTPA-CB86 was 0.49 nM.

Cell efflux studies (Figure 8C) indicated ^{99m}Tc-DTPA-CB86 has good cell retention in RAW264.7 cells, with only about 13.99% (decreased from 33.31±2.34% to 19.32± 2.01% of total input radioactivity) of ^{99m}Tc-DTPA-CB86 efflux observed from 4.5 h to 8 h incubation.

Overall, these results strongly suggested that ^{99m}Tc-DTPA-CB86 had high TSPO binding specificity, affinity in RAW264.7 cells, which warranted their further evaluation in *vivo*.

Biodistribution study

At 30, 90, and 180 min after administration, the biodistribution profiles of ^{99m}Tc-DTPA-CB86 are presented in Figure 9, ^{99m}Tc-DTPA-CB86 exhibited high levels of radioactivity accumulation in the left inflammatory ankle. At 30 min, the left inflammatory ankle uptake was 1.33±0.16 %ID/g, lower than that in the liver (5.56±0.76 %ID/g), intestine (3.48±0.59 %ID/g), stomach (2.76±0.36 %ID/g), lungs (1.51±0.14 %ID/g), and blood (1.49±0.17 %ID/g). However, the left inflammatory ankle uptake increased over time, whereas normal tissues decreased rapidly. At 90 min, the left inflammatory ankle uptake of ^{99m}Tc-DTPA-CB86 was 2.01±0.18 %ID/g, and the liver was 3.82±0.97 %ID/g, intestine 2.83±0.63 %ID/g. At 180 min, the left inflammatory ankle uptake was 2.35±0.10 %ID/g, significantly higher than the normal tissues, including the liver. Lower levels of radioactivity were always observed in muscle and bone during 30-180 min post-injection (such as 1.01±0.12 and 0.51±0.16 %ID/g at 30 min post-injection, respectively). Furthermore, ^{99m}Tc-DTPA- CB86 provided a high ratio of the left inflammatory ankle to muscle (LIA/M) and left inflammatory ankle to blood (LIA/B) (Figure 8). At 30 min, the ratio of LIA/M and LIA/B was 1.32±0.13 and 1.71±0.16, respectively. Moreover, during 90 to 180 min, the ratio of LIA/M and LIA/B increased gradually over time.

For *in vivo* blocking study (Figure 9), ^{99m}Tc-DTPA-CB86 was coinjected with a large excess (300 μg) of the unlabeled DTPA-CB86 to saturate endogenous and overexpressed TSPO. The co-injection of DTPA-CB86 reduced the uptake of ^{99m}Tc-DTPA-CB86 in several tissues including liver, lung, heart, intestine, and left inflammatory ankle, et al. (P<0.05), whereas the kidney, muscle, and bone uptake are not significantly

changed in the blocking group (P>0.05). ^{99m}Tc-DTPA-CB86 provided a high ratio of the left inflammatory ankle to muscle (LIA/M) and the left inflammatory ankle to blood (LIA/B) (Figure 9).

SPECT imaging

SPECT images acquired at 30, 90, and 180 min after injection of ^{99m}Tc-DTPA -CB86 are shown in Figure 10A. ^{99m}Tc-DTPA-CB86 accumulated in the left inflammatory ankles at 30 min and then showed a gradual increase of uptake. During 90-180 min after injection, the left inflammatory ankles were clearly visible, with good inflammatory to background contrast. When co-injected with unlabeled DTPA-CB86 (300 μg), the left inflammatory ankles was barely visible on SPECT images at 30-180 min after injection (Figure 10B). Regions of interest (ROIs) analysis of SPECT showed a high ratio of the left inflammatory ankle to muscle (LIA/M) for RA rats injected unblocking dose compared to with 300 μg blocking dose at 30-180 min post-injection (Figure 11) (P <0.05).

Evaluating therapy response of steroid anti-inflammatory therapy

In dexamethasone treated RA rats, swelling was reduced during the treatment. Clinical scores of RA rats were reduced during the drugs treatment. As shown in Figure 12, ^{99m}Tc-DTPA-CB86 accumulation in the left inflammatory ankles at 7th day and 15th day after treatment significantly decreased compared to the control group, especially at 15th day after treatment.

Histological findings

HE staining showed that synovial hyperplasia and infiltration of inflammatory cells (such as lymphocaytes and macrophages) could be detected in the left inflammatory ankles (Figure 13A), while no inflammation signs were observed in the normal contralateral ankles (Figure 13B). Immunohistochemistry (IHC) showed that positive staining of TSPO could be detected in the left inflammatory ankles (Figure 13C), while negative expression of TSPO was observed in the normal contralateral normal ankles (Figure 13B).

Discussion

Rheumatoid arthritis (RA) is a chronic systemic autoimmune inflammatory disease of unknown cause that affects over 1.0% of the population in developed countries. It may begin at any age but usually initiates between 30 and 50 years old and is approximately three-times more common in the female gender (7). RA is characterized by chronic inflammation not only mainly involving the synovium of both small and large joints, but also affecting skin, eyes, lungs, heart and blood vessels, leading to anatomical alteration and functional disability (7). The etiology of RA is very complex and is yet to be explored properly. It has a wide spectrum of clinical manifestations, variability in disease severity, progression and differences in therapeutic response. These heterogeneous phenotypes of RA may suggest that variety of factors can contribute in the development of this complex trait, which includes environmental, hormonal and genetic factors (5). Recently, mounting data of evidence suggest that macrophages play a central

role in the pathogenesis of RA, since they generate cytokines that not only initiate inflammation leading to synovitis, but also promote synovitis development contributing to destruction of cartilage and bone. Increased numbers of macrophages in the RA synovial tissue has a significant correlation with the degree of disease activity, including C-reactive protein levels, swollen joint count, synovial lining layer thickness, and joint severity (33). Numerous preclinical and clinical studies indicated that changes in numbers of synovial sublining macrophages and the expression of inflammatory products correlate with clinical improvement (33, 34). Therefore, synovial macrophages have great value as a molecular target for disease diagnosis, therapeutic intervention, and a predictive marker of the response to antirheumatic treatment. Accordingly, imaging of lesional macrophages could serve as a biomarker of disease progression and therapeutic intervention.

Imaging of RA using conventional methods such as CT and MRI provides information mainly about structural changes in the involved tissues. Thus, conventional radiography has poor sensitivity in the detection of the inflammatory process that happens in the initial stages of RA. On the other hand, nuclear medicine provides functional assessment of physiological processes using radiolabeled targeting specific elements of the inflammatory process, and therefore has significant potential for timely diagnosis and adequate follow-up of RA. Several single photon emission computed tomography (SPECT) and positron emission tomography (PET) radiopharmaceuticals have been developed and applied in this field (11). Those radiopharmaceuticals mainly include not-targeting specific tracers, such as ^{99m}Tc-MDP and ^{18}F-FDG, and targeting specific tracers, such as ^{99m}Tc-anti-CD20, ^{123}I-IL-1ra and ^{124}I-anti-CD20. Nonetheless, the pitfalls of probes including low specificity, or large size severely hamper their clinical applications (18). Furthermore, Compared with PET, SPECT held several advantages over PET including lower cost, more widespread availability. Moreover, ^{99m}Tc is an ideal radioisotope for SPECT imaging due to its favorable physical and imaging characteristics (γ ray = 140 keV, half-life = 6.02 hours), low cost and commercial availability. So, it is urgent to develop a new macrophage-targeted SPECT probe for imaging of rheumatoid arthritis.

Translocator protein (TSPO) is an 18 kDa outer mitochondrial membrane protein. In the central nervous system, TSPO becomes upregulated in activated microglia in response to central nervous system injury. In the periphery, high levels of TSPO expression have also been reported in activated macrophages in a variety of inflammatory diseases (21). Thus, TSPO is considered as a promising biomarker for inflammatory diseases. As a result, a large number of TSPO-targeted radioligands have been synthesized for PET imaging to monitor neurodegenerative diseases, neuroinflammation and peripheral inflammation including ^{11}C-PK11195, ^{11}C-DA A1106, ^{11}C-PBR28, ^{18}F-PBR06, and ^{18}F-DPA-714. PK11195 is a classic ligand of TSPO. Due to the low in vivo specific binding of ^{11}C-PK11195, recent efforts have focused on identifying novel compounds that selectively bind to TSPO with high affinity in an effort to improve the delineation of in vivo specific binding (35). In this regard, many new classes of compounds have been identified that have members that bind TSPO specifically with low nanomolar or sub-nanomolar affinity. Among these novel compounds, CB86 has been shown higher affinity (IC_{50} = 1.6 nM) compared to

PK11195 (IC_{50} = 2.2 nM) (36). In this study, we developed a ^{99m}Tc-based CB86 for TSPO imaging, and proved its targeting efficiency with in vitro and in vivo imaging.

To meet the need for quantifiable imaging targeting to TSPO sites, we focused on linear polyaminopolycarboxylic acid chelating agents as metal ions binding agents. DTPA is known as an efficient chelating agent, and has been used as an MRI contrast agent as well as radiopharmaceuticals (37). Importantly, we introduced DTPA groups to enhance the water solubility of the TSPO probe and to minimize the intrahepatic metabolism. The chelator DTPA was attached to CB86 compound via the chemical reaction between DTPA anhydride and CB86 functionalized amine under mild conditions of pH and temperatures. In this study, DTPA-CB86 was prepared successfully with more than 90% yield and labeled with ^{99m}Tc with high efficiency.

CB86 was labeled with ^{99m}Tc via DTPA by the direct labeling method, and then measured the binding specificity and affinity to TSPO. The probe ^{99m}Tc-DTPA-CB86 showed high binding affinity to the RAW264.7 cell TSPO with an IC_{50} of 0.49 nM (Fig. 8B). In vitro cell uptake experiments showed that ^{99m}Tc-DTPA-CB86 had rapid accumulation in the RAW264.7 cells, and reached a highest value of 36.45 ± 2.18% of applied activity at 180 min (Fig. 8A). The cell efflux study showed that $^{99}Tc^{m}$-DTPA-CB86 has good cell retention by RAW264.7 cells (Fig. 8A). This accumulation is TSPO specific receptor binding since the rapid cellular uptake of the tracer could be effectively blocked by cold DTPA-CB86 (Fig. 8A), suggesting that labeling has not influenced the ability of CB86 to bind specifically to TSPO. These results warranted the further evaluation of the probe for in vivo TSPO-targeted imaging.

^{99m}Tc-DTPA-CB86 showed good in vivo pharmacokinetics for TSPO targeted SPECT imaging. ^{99m}Tc-DTPA-CB86 exhibited rapid inflammatory ankle accumulation and blood clearance, which are the major advantages of using small molecules as imaging agents compared to large long circulating proteins such as full antibodies or antibody fragments (18). It rapidly localized in the left inflammatory ankles and showed good inflammatory uptake, retention, and inflammatory -to-muscle ratios (Fig. 9, 10, and 11). The left inflammatory ankles could be clearly visualized with good contrast with good contrast by SPECT at 30–180 min after injection. It is also interesting to find out that the inflammatory uptake of the ^{99m}Tc-DTPA-CB86, and inflammatory to muscle ratio are higher than those of the ^{18}F-DPA-714,^{11}C-DPA-713,and (R)-^{11}C-PK11195 (2,23). Evaluation of the probe in these RA rats demonstrated that ^{99m}Tc-DTPA-CB86 is a promising agent for TSPO imaging.

In this study, the kidney and liver showed the highest uptake because they are the major organs of metabolism. In agree with previous study (38), radioactivity was found in the lung, heart, intestine, and stomach since these normal organs have moderate TSPO expression. A high expression of the target in normal organ might appreciable influence the imaging results, especially when the target level in the lesion is low. After optimization of spiking doses was administered to saturate the target expression in normal organ, an increase lesion-normal ratio could be achieved (18,29). The in vivo TSPO binding specificity of ^{99m}Tc-DTPA-CB86 was also verified. When 300 μg of unlabeled DTPA-CB86 was co-injected,

uptakes in high TSPO expression organs/tissues, such as inflammatory ankle, lung, heart, intestine, and stomach lung, heart, intestine, and stomach, were both significantly reduced ($P < 0.05$).

According to the European League Against Rheumatism (EULAR), RA should initially be treated with synthetic disease-modifying antirheumatic drugs (DMARDs) in combination with glucocorticoids (39). Moreover, The guides underline the importance of glucocorticoids and reflect convincing evidence for their beneficial effects (39). In this study, RA rats treated with dexamethasone once a day for 2 weeks, their swelling ankles and clinical scores were reduced during the treatment. ^{99m}Tc-DTPA-CB86 accumulation in the left inflammatory ankles at 7th day and 15th day after treatment significantly decreased compared to the control group, especially at 15th day after treatment (Fig. 12). The results indicated that ^{99m}Tc-DTPA-CB86 SPECT may real-time monitor therapy response of anti-inflammatory therapy.

Conclusion

This study demonstrates that ^{99m}Tc-DTPA-CB86 SPECT imaging can identify the activated macrophages in the synovial joints in RA rat models and monitor therapy response of anti-inflammatory therapy. ^{99m}Tc-DTPA-CB86 SPECT may be a useful biomarker as a non-invasive imaging method for clinical management of RA.

Abbreviations

TSPO: Translocator protein; PET: Positron emission tomography; SPECT: Single photon emission computed tomography; ^{99m}Tc: ^{99m}Technetium; RA: Rheumatoid arthritis; CFA: Complete Freund's Adjuvant; ACR: American College of Rheumatology; EULAR: European League Against Rheumatism; CRP: C-reactive protein; ESR: Erythrocyte sedimentation rate; RF: Rheumatoid factor; ACCP: Anti-citrullinated protein antibodies; CT: Computed tomography; MRI: Magnetic resonance imaging; ^{18}F-FDG: ^{18}F-Fluoro deoxy-glucose; PBR: Peripheral-type benzodiazepine receptor; DTPAA: Diethylenetriamine-pentaacetic acid anhydride; PMSF: Phenylmethanesulfonyl fluoride; LPS: Lipopolysaccharide; DMEM: PBS: Phosphate-buffered saline; DMSO: Dimethylsulfoxide; FBS: Fetal bovine serum; HPLC: High-performance liquid chromatography; qRT-PCR: Quantitative Real-Time PCR; MBq: Megabecquerel; mCi: MilliCuries; mg/dL: Milligrams per deciliter; mL: Milliliters; µL: Microliters; %ID/g: Percentage of the injected radioactivity per gram of tissue; LIA/B: The radioactivity ratios of the left inflammatory ankle to blood; LIA/M: The left inflammatory ankle to muscle; ROIs: Regions of interest; HE: Hematoxylin and Eosin; IHC: Immunohistochemistry

Declarations

Acknowledgements

Not applicable.

Authors' contributions

PL, RY and FS coordinated the study, acquired and interpreted data and performed the statistical analyses. ZY and WD participated in coordination of the study, and acquired data. ZG participated in the design and performance the statistical analyses. CM performed the statistical analyses. HL and WW participated in the design and coordination of the study, interpreted data, and helped draft the manuscript. XH conceived, designed and conducted the study, drafted the manuscript. All authors read and approved the final manuscript.

Funding

This work was supported by grants from the National Natural Science Foundation of China (NSFC) (81571707), and Fujian medical innovation project (2019-CXB-32).

Availability of data and materials

The datasets used and/or analyzed during the current study are available from the corresponding author on reasonable request.

Ethics approval and consent to participate

All procedures were approved by the Institutional Animal Care and Use Committee of Zhongshan Hospital Xiamen University.

Consent for publication

Not applicable.

Competing interests

The authors declare that they have no competing interests.

Author details

1. Department of Nuclear Medicine, Zhongshan Hospital Xiamen University, 201 Hubin South Road, Xiamen, Fujian, 361004, China.
2. Center for Molecular Imaging and Translational Medicine, Xiamen University, Xiang'an South Road Xiamen, Fujian, 361005 China.
3. Department of Health Medicine, Zhongshan Hospital Xiamen University, 201 Hubin South Road, Xiamen, Fujian, 361004, China.

References

1. Ferro F, Elefante E, Luciano N, Talarico R, Todoerti M. One year in review 2017: novelties in the treatment of rheumatoid arthritis. Clin Exp Rheumatol. 2017; 35(5): 721-734.
2. Pottier G, Bernards N, Dollé F, Boisgard R. [18F]DPA-714 as a biomarker for positron emission tomography imaging of rheumatoid arthritis in an animal model. Arthritis Res Ther. 2014; 16(2):R69.
3. Itoh Y. Metalloproteinases: potential therapeutic targets for rheumatoid arthritis. Endocr Metab Immune Disord Drug Targets. 2015;15(3):216-222.
4. Minichiello E, Semerano L, Boissier MC. Time trends in the incidence, prevalen- ce, and severity of rheumatoid arthritis: A systematic literature review. Joint Bone Spine. 2016. pii: S1297-319X(16)30129-4.
5. Jalil SF, Arshad M, Bhatti A, Ahmad J, Akbar F, Ali S, John P. Rheumatoid arthritis: What have we learned about the causing factors? Pak J Pharm Sci. 2016; 29(2): 629-645.
6. Ummarino D. Rheumatoid arthritis: Smoking influences autoimmunity to vime- ntin. Nat Rev Rheumatol. 2016; 12(11):624.
7. De Cata A, D'Agruma L, Tarquini R, Mazzoccoli G. Rheumatoid arthritis and the biological clock. Expert Rev Clin Immunol. 2014;10(5):687-695.
8. Márquez A, Martín J, Carmona FD. Emerging aspects of molecular biomarkers fo- r diagnosis, prognosis and treatment response in rheumatoidarthritis. Expert Rev Mol Diagn. 2016; 16(6):663-675.
9. Sparks JA. Rheumatoid Arthritis. Ann Intern Med. 2019;170(1): ITC1-ITC16.
10. Gotthardt M, Bleeker-Rovers CP, Boerman OC, Oyen WJ. Imaging of inflammati- on by PET, conventional scintigraphy, and other imaging techniques. J Nucl Med Technol. 2013; 41(3):157-169.
11. Rosado-de-Castro PH, Lopes de Souza SA, Alexandre D, Barbosa da Fonseca LM, Gutfilen B. Rheumatoid arthritis: Nuclear Medicine state-of-the-art imaging. World J Orthop. 2014; 5(3):312-318.
12. Soler Palacios B, Estrada-Capetillo L, Izquierdo E, Criado G, Nieto C, Municio C, González-Alvaro I, Sánchez-Mateos P, Pablos JL, Corbí AL, Puig-Kröger A. Macrophages from the synovium of active rheumatoid arthritis exhibit an activen A-dependent pro-inflammatoryprofile. J Pathol. 2015; 235(3):515-526.
13. Arthur JS, Ley SC.Mitogen-activated protein kinases in innate immunity. Nat Rev Immunol. 2013;13(9):679-692.
14. Udalova IA, Mantovani A, Feldmann M. Macrophage heterogeneity in the context of rheumatoid arthritis. Nat Rev Rheumatol. 2016;12(8):472-485.
15. Malviya G, Anzola KL, Podestà E, Laganà B, Del Mastro C, Dierckx RA, Scopi- naro F, Signore A. (99m)Tc-labeled rituximab for imaging B lymphocyte infiltration in inflammatory autoimmune disease patients. Mol Imaging Biol. 20 12;14 (5):637-646.
16. Barrera P, van der Laken CJ, Boerman OC, Oyen WJ, van de Ven MT, van Lent PL, van de Putte LB, Corstens FH. Radiolabelled interleukin-1 receptor antago- nist for detection of synovitis in patients with rheumatoid arthritis. Rheumatolog- y (Oxford). 2000;39(8):870-874.
17. Tran L, Huitema AD, van Rijswijk MH, Dinant HJ, Baars JW, Beijnen JH, Vogel WV. CD20 antigen imaging with 124I-rituximab PET/CT in patients with rheumatoid arthritis. Hum Antibodies. 2011;20(1-2):29-35.
18. Su X, Cheng K, Liu Y, Hu X, Meng S, Cheng Z. PET imaging of insulin-like growth factor type 1 receptor expression with a 64Cu-labeled Affibody molecule. Amino Acids. 2015;47(7):1409-1419.

19. Papadopoulos V, Baraldi M, Guilarte TR, Knudsen TB, Lacapère JJ, Lindemann P, Norenberg MD, Nutt D, Weizman A, Zhang MR, Gavish M. Translocator prot- ein (18kDa): new nomenclature for the peripheral-type benzodiazepine receptor based on its structure and molecular function. Trends Pharmacol Sci. 2006; 27(8): 402-409.
20. Guo Y, Kalathur RC, Liu Q, Kloss B, Bruni R, Ginter C, Kloppmann E, Rost B, Hendrickson WA. Protein structure. Structure and activity of tryptophan-rich TS- PO proteins. Science. 2015; 347(6221):551-555.
21. Kanegawa N, Collste K, Forsberg A, Schain M, Arakawa R, Jucaite A, Lekander M, Olgart Höglund C, Kosek E, Lampa J, Halldin C, Farde L, Varrone A, Cerven- ka S. In vivo evidence of a functional association between immune cells in blood and brain in healthy human subjects. Brain Behav Immun. 2016;54:149-157.
22. Gatliff J, Campanella M. TSPO: kaleidoscopic 18-kDa amid biochemical pharm- acology, control and targeting of mitochondria. Biochem J. 2016;473(2):107-121.
23. Gent YY, Weijers K, Molthoff CF, Windhorst AD, Huisman MC, Kassiou M, Jans- en G, Lammertsma AA, van der Laken CJ. Promising potential of new generatio- n translocator protein tracers providing enhanced contrast of arthritisimaging by positron emission tomography in a rat model of arthritis. Arthritis Res Ther. 2014; 16(2):R70.
24. Gent YY, Ahmadi N, Voskuyl AE, Hoetjes N, van Kuijk C, Britsemmer K, Turks- tra F, Boers M, Hoekstra OS, van der Laken CJ. Detection of subclinical syno- vitis with macrophage targeting and positron emission tomography in patients with rheumatoid arthritis without clinical arthritis. J Rheumatol. 2014;41 (11): 21 45-2152.
25. Zhang Y, Liu P, Jiang Y, Dou X, Yan J, Ma C, Fan Q, Wang W, Su F, Tang H, Su X. High Expression of Neuropilin-1 Associates with Unfavorable Clinico- pathological Features in Hepatocellular Carcinoma. Pathol Oncol Res. 2016; 22 (2):367-375.
26. Su X, Chen Q, Chen W, Chen T, Li W, Li Y, Dou X, Zhang Y, Shen Y, Wu H, Yu C. Mycoepoxydiene inhibits activation of BV2 microglia stimulated by lipopolysaccharide through suppressing NF-κB, ERK 1/2 and toll-like receptor pathways. Int Immunopharmacol. 2014; 19(1):88-93.
27. Dou X, Yan J, Zhang Y, Liu P, Jiang Y, Lv S, Zeng F, Chen X, Wang S, Zhang H, Wu H, Zhang H, Ouyang L, Su X. SPECT imaging of neuropilin receptor type-1 expression with 131I-labeled monoclonal antibody. Int J Oncol. 2016; 49(3):96 1-970.
28. Guo Z, Gao M, Song M, Shi C, Zhang P, Xu D, You L, Zhuang R, Su X, Liu T, Du J, Zhang X. Synthesis and Evaluation of (99m)Tc-Labeled Dimeric Folic Acid for FR-Targeting. Molecules. 2016; 21(6). pii: E817.
29. Su X, Cheng K, Jeon J, Shen B, Venturin GT, Hu X, Rao J, Chin FT, Wu H, Cheng Z. Comparison of two site-specifically (18)F-labeled affibodies for PET imaging of EGFR positive tumors. Mol Pharm 11:3947-3956, 2014.
30. Li C, Feng H, Xia X, Wang L, Gao B, Zhang Y, Lan X. (99m) Tc-labeled tetramer and pentamer of single-domain antibody for targeting epidermal growth factor receptor in xenografted tumors. J Labelled Comp Radiopharm. 2016; 59(8):305- 312.
31. Teixeira V, Fernández M, Oddone N, Zhang X, Gallazzi F, Cerecetto H, Gambini JP, Porcal W, Cabral P, Quinn TP. The Effect of A Hexanoic Acid Linker Insertion on the Pharmacokinetics and Tumor Targeting Properties of the Melanoma Imaging Agent 99mTc-HYNIC-cycMSH. Anticancer Agents Med Chem.

2017;17(8):1144-1152.
32. Chen L, Bao B, Wang N, Xie J, Wu W. Oral Administration of Shark Type II Col- agen Suppresses Complete Freund's Adjuvant-Induced RheumatoidArthritis in Rats. Pharmaceuticals (Basel). 2012;5(4):339-352.
33. Choi S, You S, Kim D, Choi SY, Kwon HM, Kim HS, Hwang D, Park YJ, Cho CS, Kim WU.Transcription factor NFAT5 promotes macrophage survival in rheumatoid arthritis. J Clin Invest. 2017; 127(3):954-969.
34. Haringman JJ, Gerlag DM, Zwinderman AH, Smeets TJ, Kraan MC, Baeten D, McInnes IB, Bresnihan B, Tak PP. Synovial tissue macrophages: a sensitive biomarker for response to treatment in patients with rheumatoid arthritis. Ann Rheum Dis. 2005;64(6):834-838
35. Venneti S, Lopresti BJ, Wiley CA. Molecular imaging of microglia/macrophages in the brain. Glia. 2013;61(1):10-23.
36. Laquintana V, Denora N, Musacchio T, Lasorsa M, Latrofa A, Trapani G. Peripheral Benzodiazepine Receptor ligand–PLGA polymer conjugates potentially useful as delivery systems of apoptotic agents. J Control Release. 2009;137(3):185-195.
37. Xia X, Feng H, Li C, Qin C, Song Y, Zhan Y, Lan X. 99mTc-labeled estradiol as an estrogen receptor probe: Preparation and preclinical evaluation. Nucl Med Biol. 2016;43(1):89-96.
38. Banati RB, Middleton RJ, Chan R, Hatty CR, Wai-Ying Kam W, Quin C, Graeber MB, Parmar A, Zahra D, Callaghan P, Fok S, Howell NR, Gregoire M,Szabo A, Pham T, Davis E, Liu GJ. Positron emission tomography and functional characterization of a complete PBR/TSPO knockout. Nat Commun. 2014;5: 5452.
39. Strehl C, Bijlsma JW, de Wit M, Boers M, Caeyers N, Cutolo M, Dasgupta B, Dixon WG, Geenen R, Huizinga TW, Kent A, de Thurah AL, Listing J, Mariette X, Ray DW, Scherer HU, Seror R, Spies CM, Tarp S, Wiek D, Winthrop KL, Buttgereit F. Defining conditions where long-term glucocorticoid treatment has an acceptably low level of harm to facilitate implementation of existing recommendations: viewpoints from a EULAR task force. Ann Rheum Dis 2016;75(6):952-957.

Figures

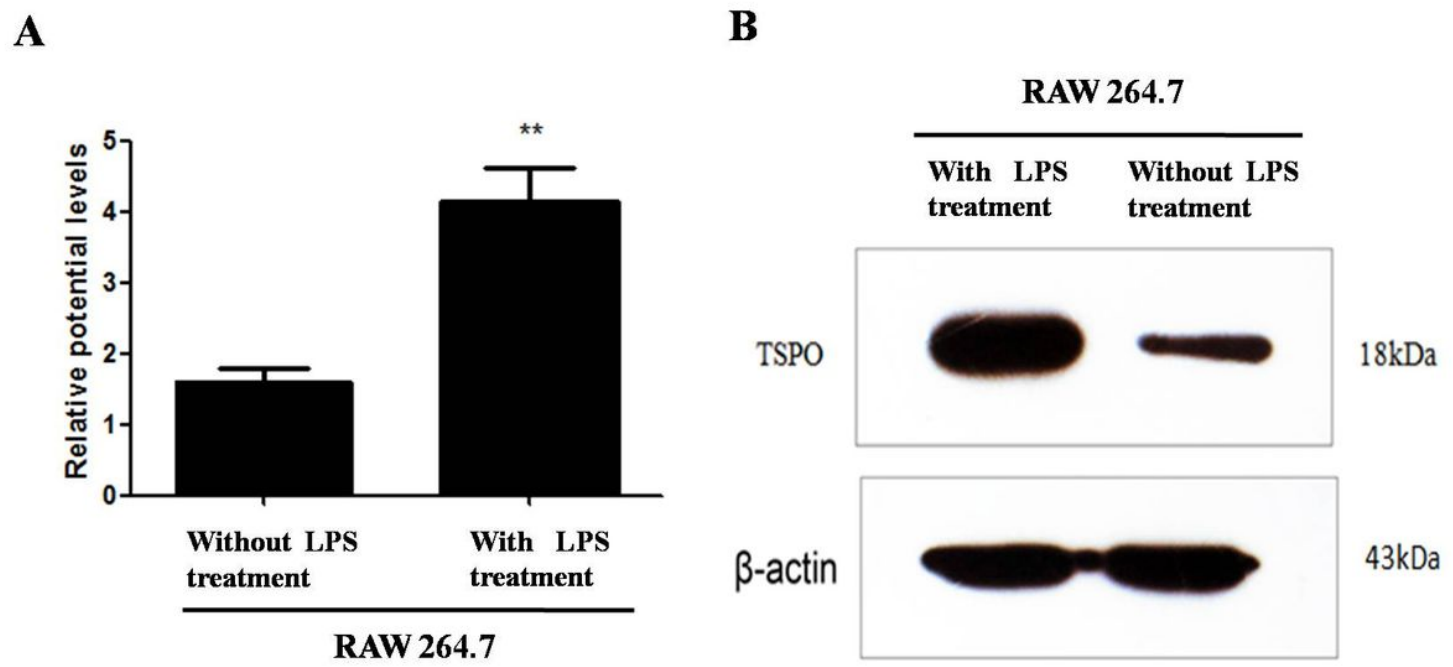

Figure 1

The expression of TSPO in the activated RAW264.7 cells was determined by qRT-PCR (A) and Western blot (B).

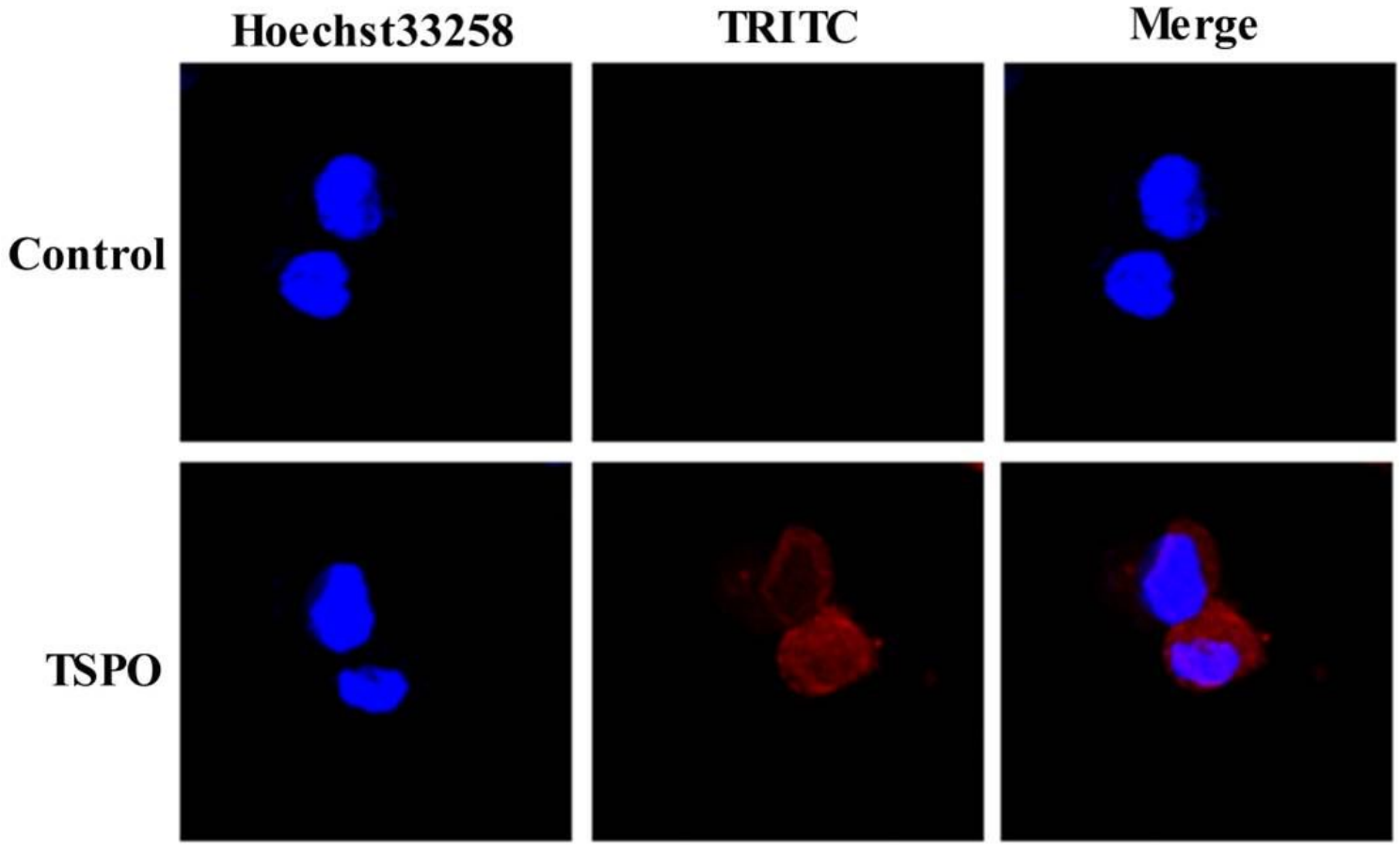

Figure 2

The immunofluorescence of the activated RAW264.7 cells.

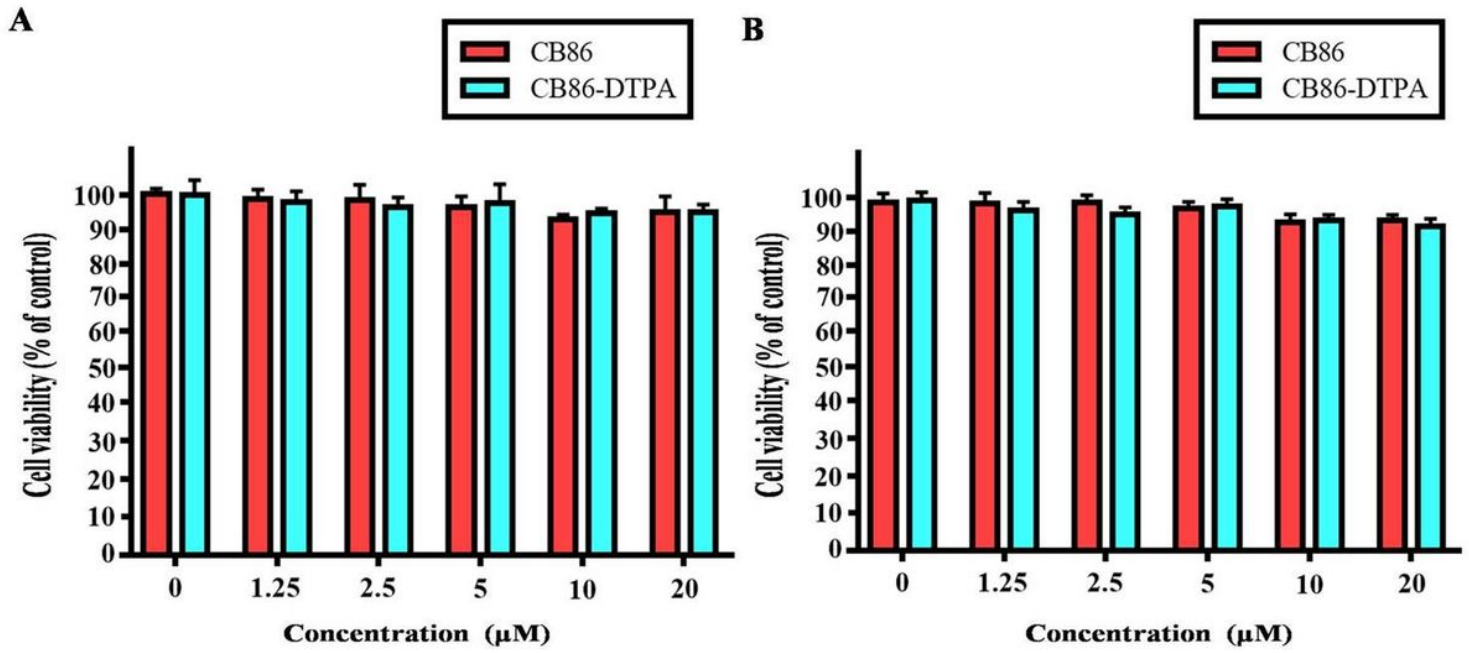

Figure 3

Cell viability values (%) of RAW264.7 cells (A) and 4T1 cells (B) after 24 hours incubation with different concentrations of CB86 and CB86-DTPA , respectively (n =3).

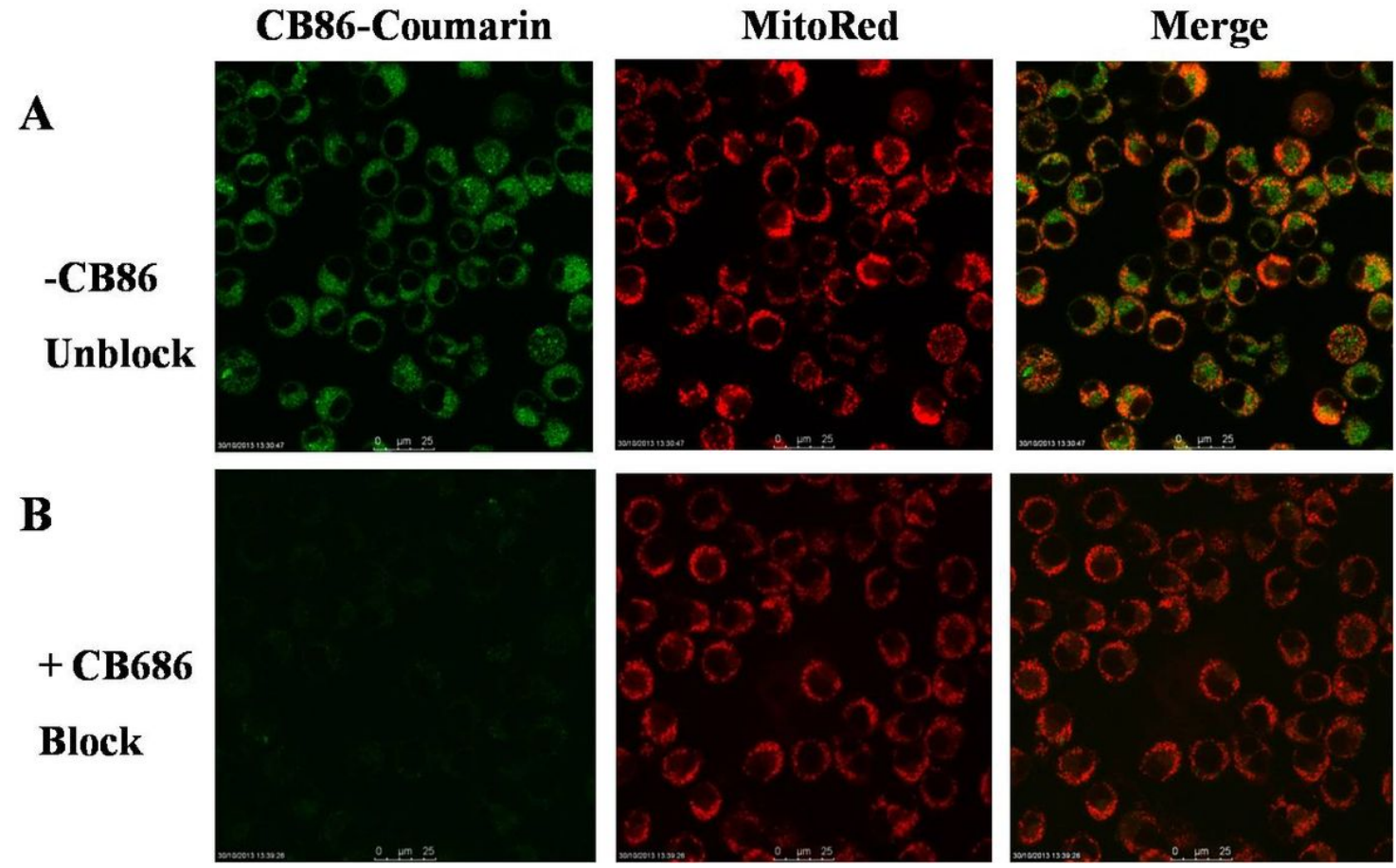

Figure 4

Fluorescence imaging of CB86 in the activated RAW264.7 cells. The activated RAW264.7 cells were stained with MitoRed and CB86-coumarin, and observed with a confocal fluorescence microscope. The distribution of CB86-coumarin (left, green), MitoRed (center, red), and the merged image (right) of the same field are shown.

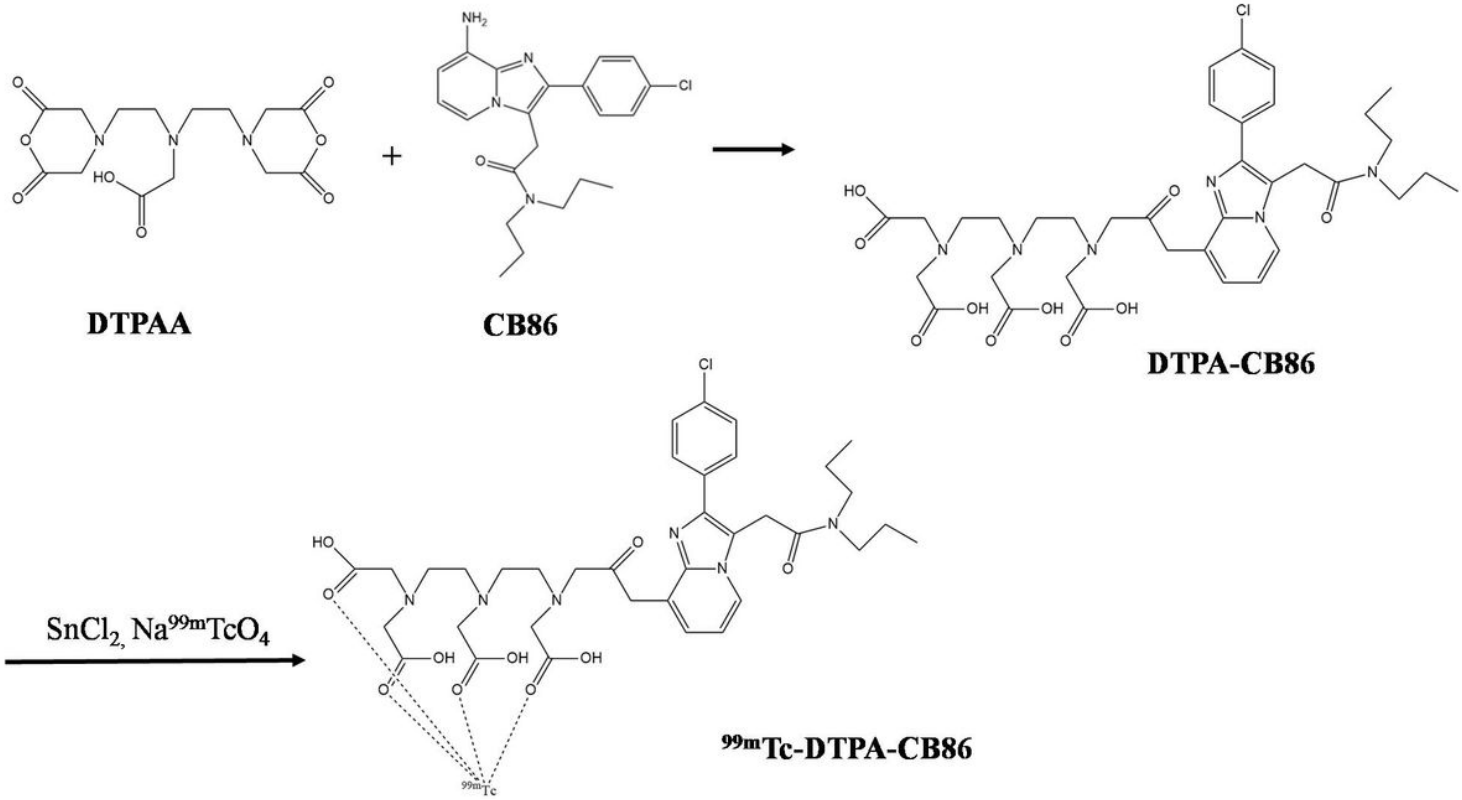

Figure 5

Synthetic scheme of 99mTc-DTPA-CB86

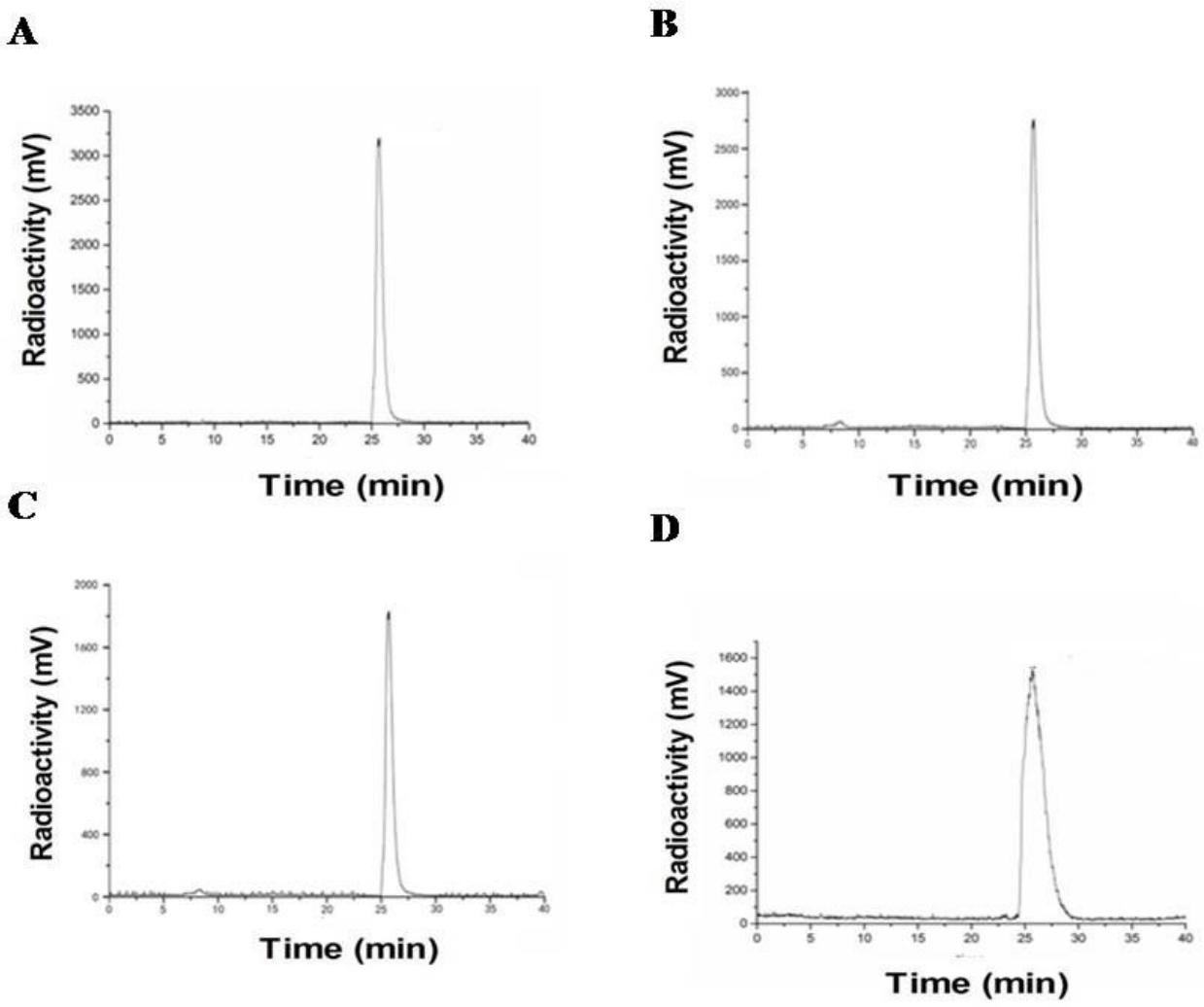

Figure 6

HPLC radiochromatograms of purified 99mTc-DTPA-CB86 (A) and radiolabeled probe after 1 h (B), 2 h (C), and 4 h (D) of incubation with PBS.

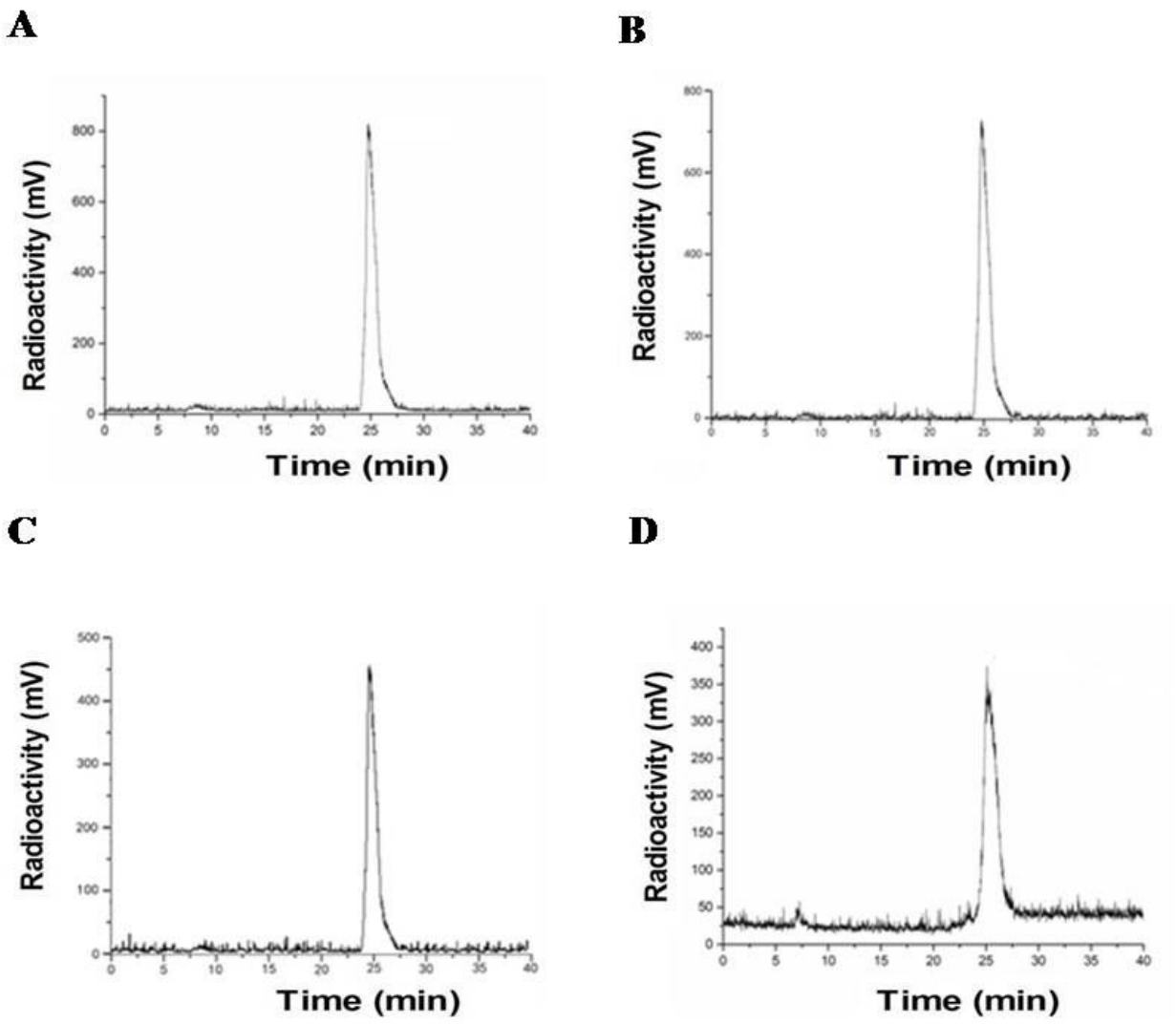

Figure 7

HPLC radiochromatograms of purified 99mTc-DTPA-CB86 (A) and radiolabeled probe after 1 h (B), 2 h (C), and 4 h (D) of incubation with mouse serum.

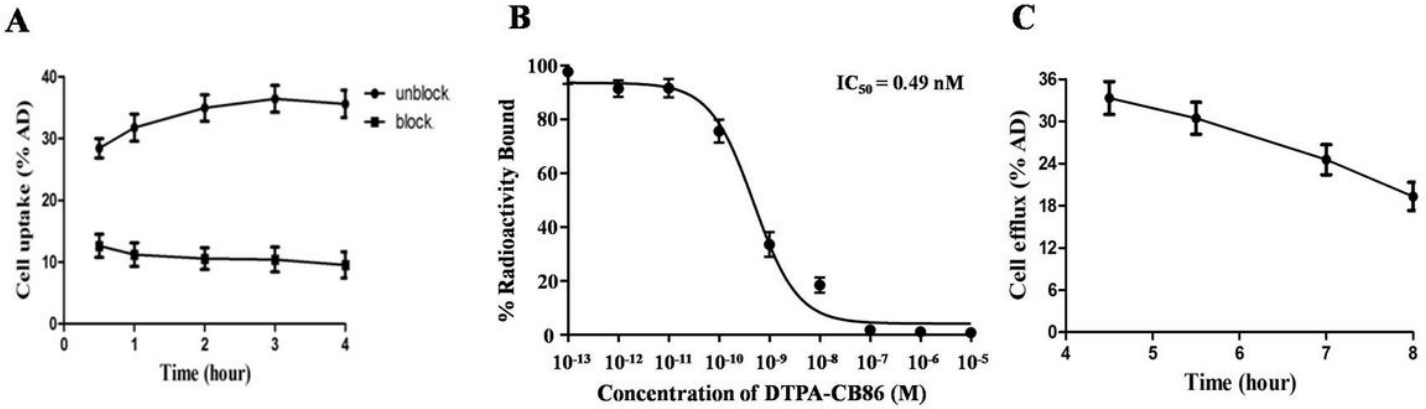

Figure 8

Uptake (A), binding affinity (B) and efflux assay (C) of 99mTc-DTPA-CB86 in RAW264.7 cells.

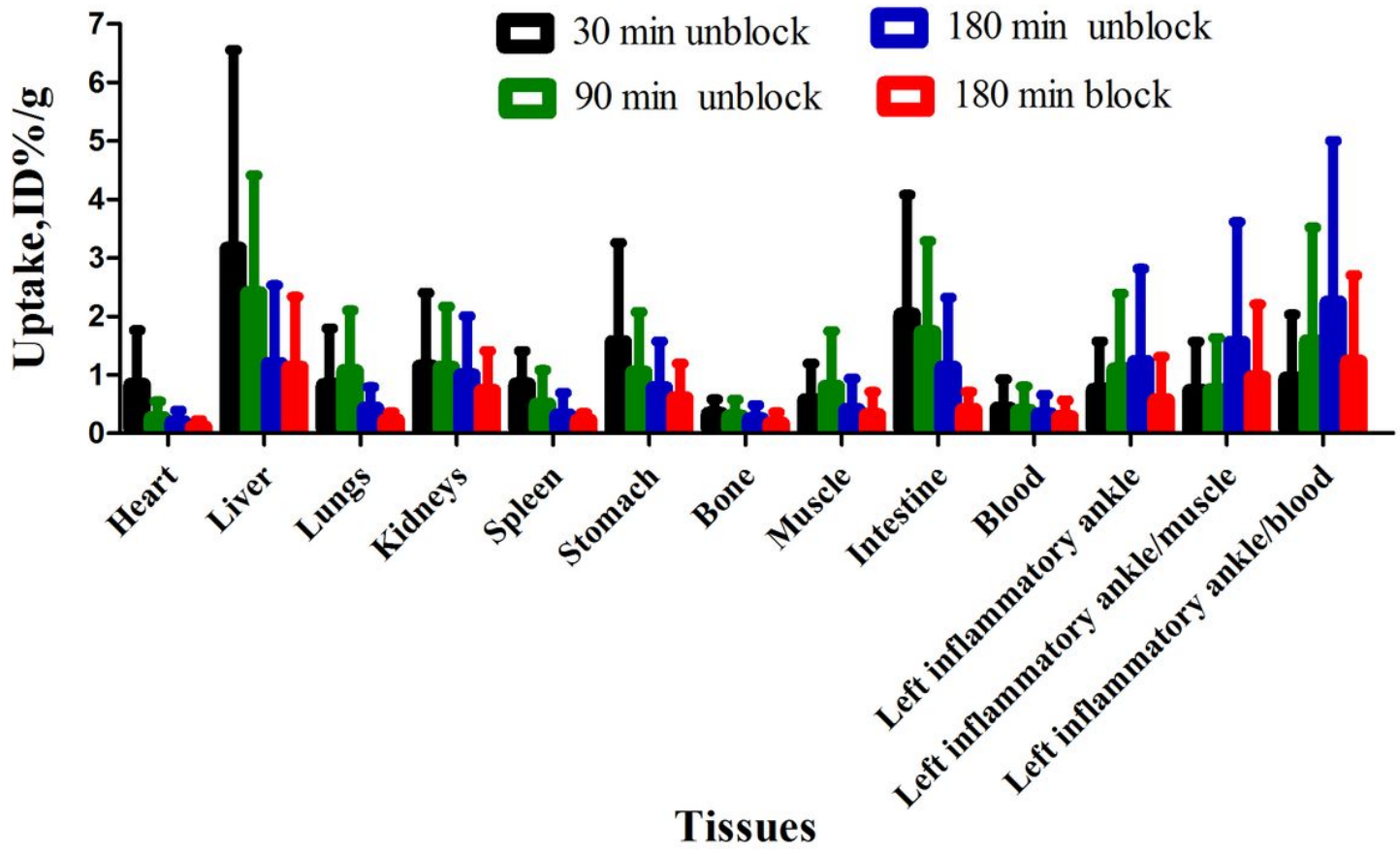

Figure 9

Biodistribution results for 99mTc-DTPA-CB86 in RA rats. Data are expressed as %ID/g at various times after intravenous injection of 99mTc-DTPA-CB86 (n = 4 for each group).

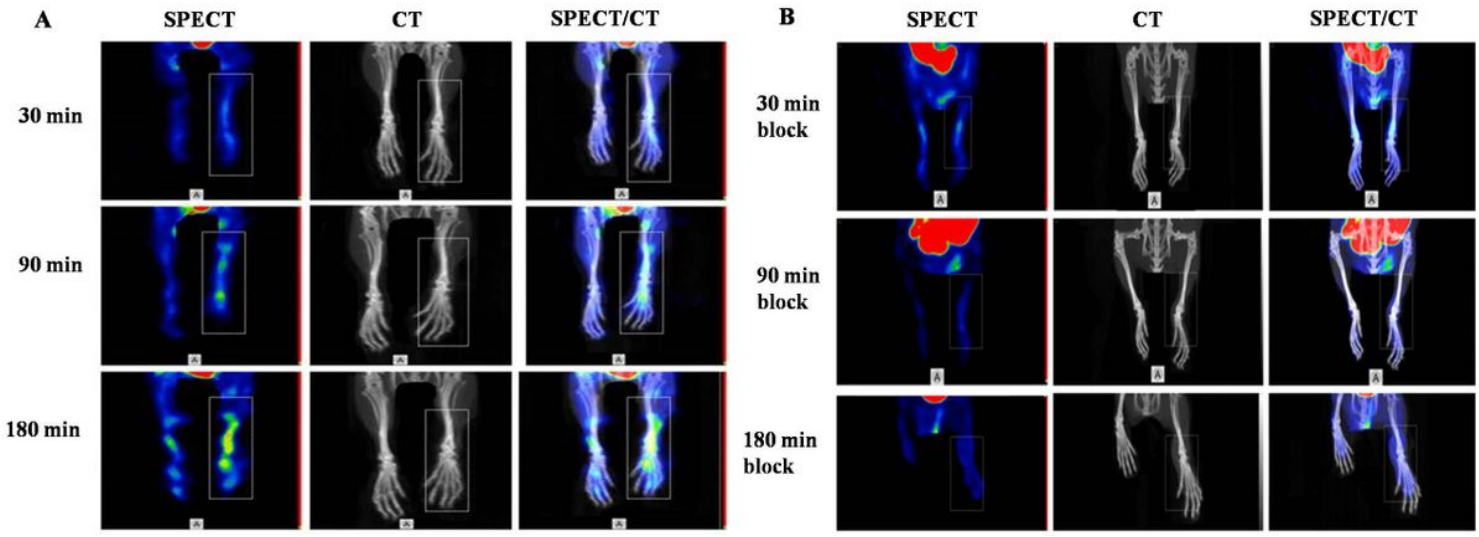

Figure 10

SPECT/CT imaging of 99mTc-DTPA-CB86 in RA rat models co- injected with 0 μg dose (unblock, A) and 300 μg dose (block, B) of DTPA-CB86 at 30,90, and 180 min after injection (n = 4 for each group).

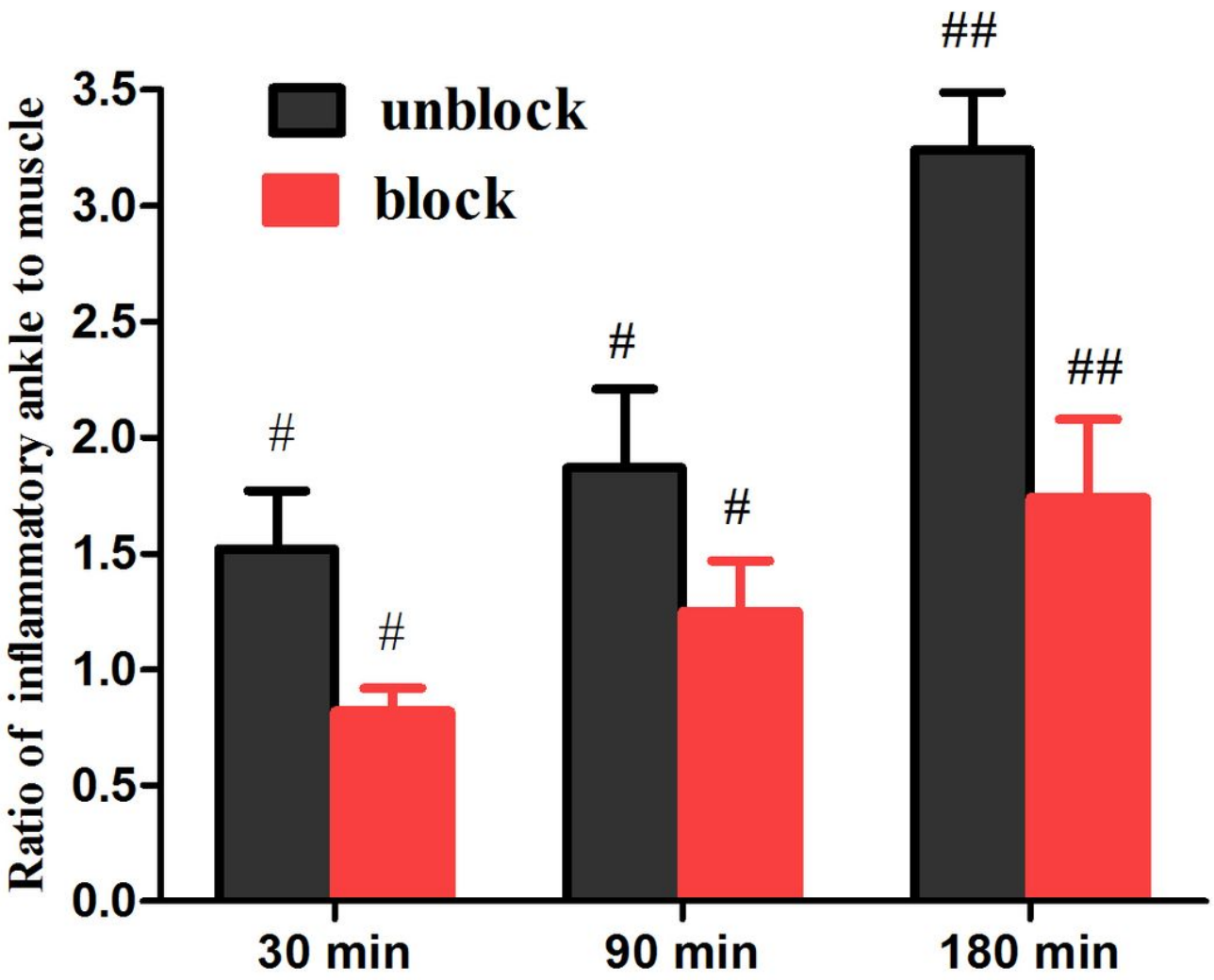

Figure 11

The ratio of the left inflammatory ankle to muscle based on SPECT imaging between 0 μg (unblock) and 300 μg (block) of dose at various times after injection with 99mTc-DTPA-CB86. (#P < 0.05, ##P < 0.01)

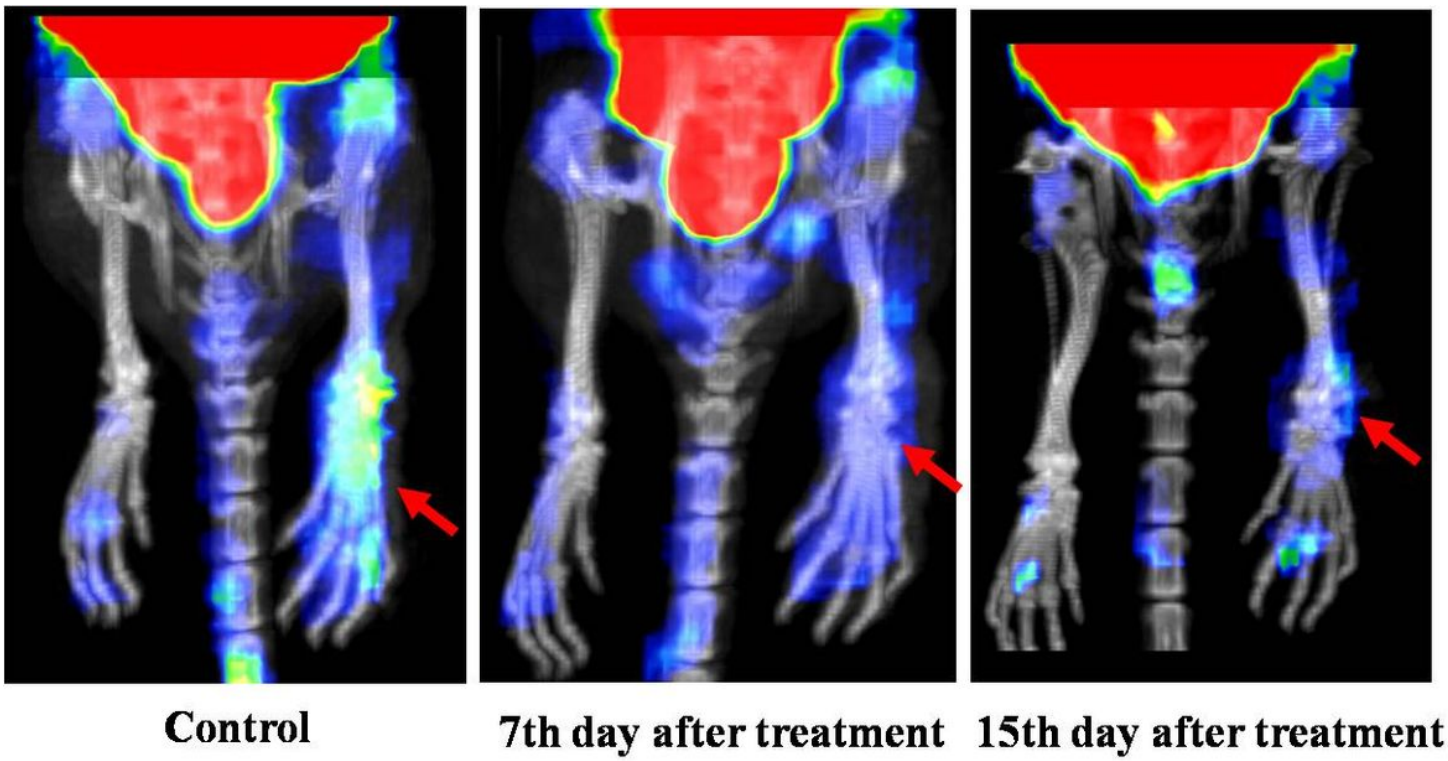

Figure 12

SPECT/CT imaging of 99mTc-DTPA-CB86 for initially evaluating the treatment response of steroid anti-inflammatory therapy.

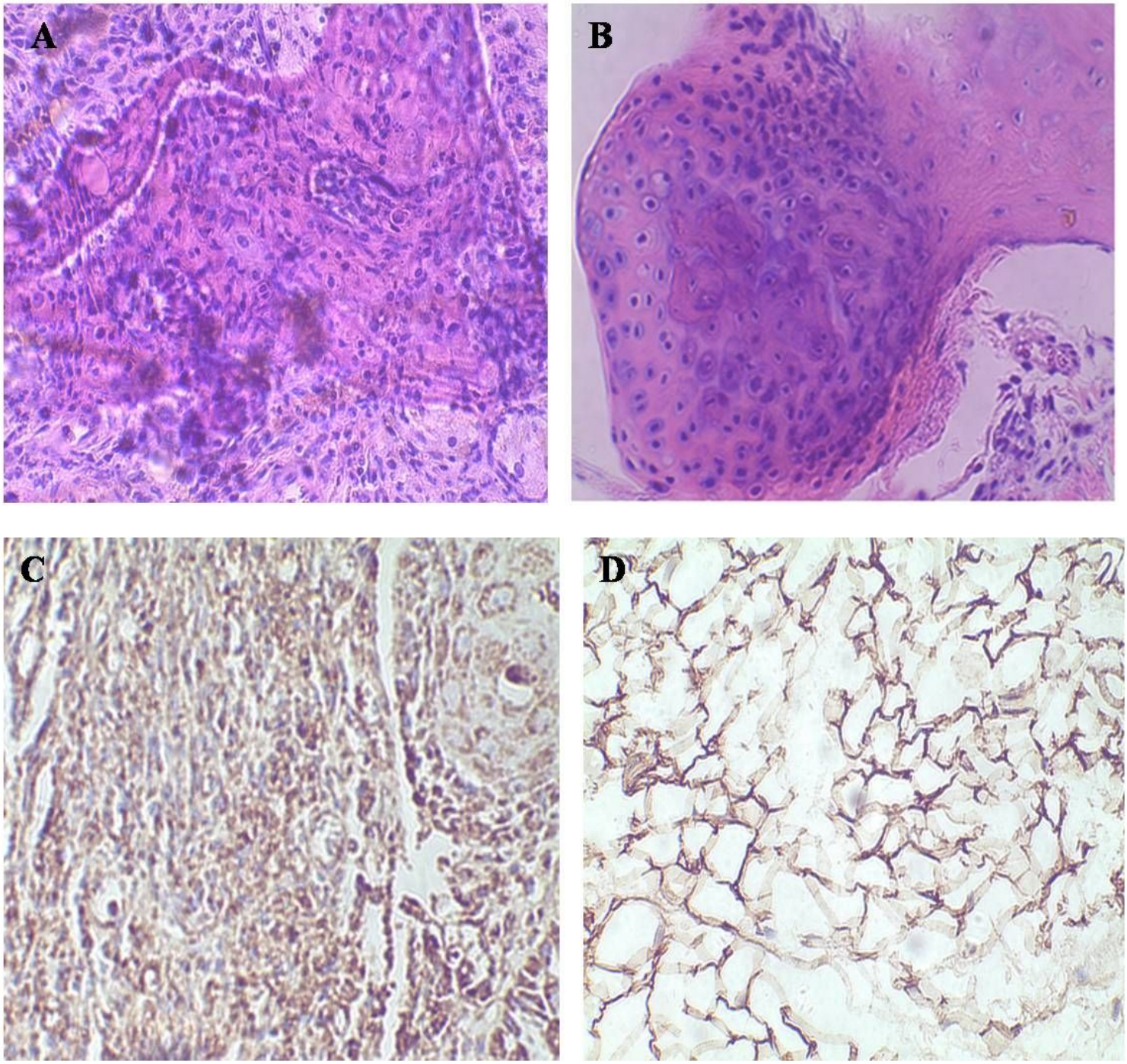

Figure 13

The findings of HE staining (A,B) and immunohistochemistry (C,D) in the left inflammatory ankles (A,C) and normal contralateral ankles (B,D) (x100). HE staining showed that synovial hyperplasia and infiltration of inflammatory cells could be detected in the left inflammatory ankles (A), while no inflammation signs were observed in the normal contralateral ankles (B). Immunohistochemistry (IHC) showed that positive staining of TSPO could be detected in the left inflammatory ankles (C), while negative expression of TSPO was observed in the normal contralateral ankles (D).